SATELLITE ORBIT ESTIMATION USING EARTH MAGNETIC FIELD MEASUREMENTS

Mohammad Nizam Filipski, Renuganth Varatharajoo
Department of Aerospace Engineering, Universiti Putra Malaysia, 43400 Serdang, Selangor D.E., Malaysia
Email: nizam@eng.upm.edu.my

ABSTRACT

This paper presents the design of an estimation algorithm for the determination of a low-Earth satellite orbit based only on the measurements of the Earth magnetic field. The algorithm is based on the extended Kalman filter (EKF) and the measure of the magnitude of the magnetic field, which provides an estimation method independent of the satellite attitude. The satellite orbit is described with a state vector formed by the classical Keplerian orbital elements. The simulation test resulted in an accurate estimation of the state vector components and yielded only a few kilometres error on the satellite position. The effect of the variation of the orbit inclination and eccentricity on the filter performances was also investigated.

Keywords: *Orbit Estimation, Extended Kalman Filter, Magnetic Field Measurements*

INTRODUCTION

The issue of determining the satellite position on its orbit with the greatest possible accuracy has been investigated since the 1960s. Today's systems of orbit determination provide position errors at the meter level and even at the centimetre level for some very specific missions like TOPEX/Poseidon [1] or GFO [2] satellites. However that degree of accuracy is not attainable without the support of some system external to the satellite: mainly Earth based stations using Satellite Laser Ranging or a combination of radar and optical sensors, and Global Positioning System (GPS). Autonomous orbit estimation methods, that do not rely on equipments other than those available onboard the satellite, have the advantages of being more reliable, less costly to operate and less vulnerable in hostile environment (jamming, loss of Earth station). One way to achieve this autonomy is to use magnetometers to measure the Earth magnetic field, which is a function of time and position. This function is well known and can easily be modelled onboard to compute the magnetic field at the satellite assumed position [3,4]. The difference between the computed and the measured magnetic field is a function of the error made in the satellite position. It is possible to determine both the orbital position and the attitude of a satellite from only the Earth magnetic field, with rate data available [5,6] or without [7-9]. The magnitude of the Earth magnetic field is sufficient to determine the satellite position. Greater accuracy can be achieved if we also know the vector direction but this requires the knowledge of the satellite attitude and is computationally more expensive [6]. In this paper we present an algorithm based on the EKF using only the magnitude of the Earth magnetic field to estimate both the satellite position and its rate of rotation. The influence of the orbit inclination and eccentricity on the efficiency of the filter is assessed through simulations.

ORBIT DYNAMICS

The satellite position is described by the classical Keplerian orbital elements (a, e, i, Ω, ω, ν). The semi-major axis a and the eccentricity e define the shape of the orbit. The inclination i, the right ascension of the ascending node Ω and the argument of perigee ω define the orientation of the orbit with respect to an inertial reference frame. The last element is the true anomaly; it defines the satellite position on the orbit with respect to the periapsis.

The simplest and also least realistic way to model the satellite movement on its orbit is to assume that the only force acting on the satellite is the gravitational attraction from the Earth, which is represented as a perfect sphere of uniform density. The most influential forces neglected in this model, for a low-Earth orbit (LEO) satellite, are caused by the Earth's atmosphere and the Earth's gravitational field. The variation of the true anomaly s is given [10] (in Ref. 10, Chap. 1) by

$$\dot{\nu} = \sqrt{\frac{\mu}{a^3}} \frac{(1+e\cos\nu)^2}{(1-e^2)^{3/2}} \tag{1}$$

where μ is the Earth's gravitational parameter. The other Keplerian orbital elements are not varying with time.

EKF ALGORITHM DESCRIPTION

For the model described in the previous paragraph it is sufficient to use the Keplerian orbital elements to represent the state of the system:

$$\boldsymbol{x}(t) = [\, a, e, i, \Omega, \omega, \nu \,]^{\mathrm{T}} \tag{2}$$

The dynamics of the orbit model is described by the following stochastic differential equation:

$$\dot{\boldsymbol{x}}(t) = \boldsymbol{f}[\boldsymbol{x}(t), t\,] + \boldsymbol{G}(t)\boldsymbol{w}(t) \tag{3}$$

with initial condition $\boldsymbol{x}(t_0)$, a Gaussian random vector with mean $\hat{\boldsymbol{x}}_0$ and covariance $\boldsymbol{P}_0$. The noise $\boldsymbol{w}(t)$ is a zero-mean white Gaussian signal, independent of $\boldsymbol{x}(t_0)$ and of strength $\boldsymbol{Q}(t)$. The matrix $\boldsymbol{G}(t)$ is the noise input matrix.
The state function is nonlinear but still simple as only the last element is different from zero:

$$\boldsymbol{f}[\boldsymbol{x}(t), t\,] = [0,0,0,0,0, \frac{\sqrt{\mu}(1+e\cos\nu)^2}{(a(1-e^2))^{3/2}}]^{\mathrm{T}} \tag{4}$$

The measurement model of the Earth's magnetic field measurement process onboard the satellite is represented by the nonlinear discrete stochastic equation,

$$\boldsymbol{z}(t_{\mathrm{k}}) = \boldsymbol{h}[\boldsymbol{x}(t_{\mathrm{k}}), t_{\mathrm{k}}\,] + \boldsymbol{v}(t_{\mathrm{k}}) \tag{5}$$

Measurements are corrupted by the noise $\boldsymbol{v}(t_{\mathrm{k}})$, a zero-mean white Gaussian vector, independent of $\boldsymbol{x}(t_0)$ and $\boldsymbol{w}(t)$, and of strength $\boldsymbol{R}(t_{\mathrm{k}})$ for all t_{k}.
The measurement function is the norm of the Earth's magnetic field vector, which value is expressed in the Earth-centered, Earth-fixed coordinate system,

$$\boldsymbol{h}[\boldsymbol{x}(t_{\mathrm{k}}), t_{\mathrm{k}}\,] = \mathrm{N}[\boldsymbol{B}(\boldsymbol{x}(t_{\mathrm{k}}), t_{\mathrm{k}})] \tag{6}$$

where $\mathrm{N}[.]$ is the norm operator.

The EKF algorithm works in a two-stage process: from some initial orbital elements the state is propagated to the nearest measurement time where it is updated by using the information from the Earth's magnetic field. Then it is propagated again until the next measurement (Figure(1)). The notation used to indicate the position of a quantity with respect to the time t_{k} is: just before t_{k}, $\boldsymbol{x}(t_{\mathrm{k}}^{-}) = \boldsymbol{x}_{\mathrm{k-1|k}}$, and just after t_{k}, $\boldsymbol{x}(t_{\mathrm{k}}^{+}) = \boldsymbol{x}_{\mathrm{k|k}}$.

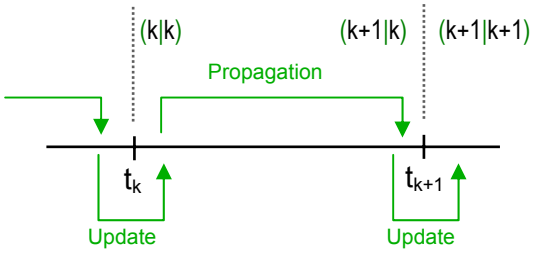

Figure 1: Stages of the Kalman filter algorithm.

Measurement Update Stage

The state is updated according to the following equations [11]

$$\hat{\boldsymbol{x}}_{k|k} = \hat{\boldsymbol{x}}_{k|k-1} + \boldsymbol{K}_k \{z_k - \hat{z}_{k|k-1}\} \tag{7}$$

where $\hat{z}_{k|k-1} = \boldsymbol{h}[\hat{\boldsymbol{x}}_{k|k-1}, t_k] = \mathrm{N}[\boldsymbol{B}(\hat{\boldsymbol{x}}_{k|k-1}, t_k)]$ is the best estimate of the measurement available before the time t_k. The matrix $\boldsymbol{K}_k$ (a 6×1 matrix in this filter) is the Kalman gain and it is equal to

$$\boldsymbol{K}_k = \boldsymbol{P}_{k|k-1}\boldsymbol{H}_{k|k-1}^{\mathrm{T}} \left[\boldsymbol{H}_{k|k-1}\boldsymbol{P}_{k|k-1}\boldsymbol{H}_{k|k-1}^{\mathrm{T}} + \boldsymbol{R}_k\right]^{-1} \tag{8}$$

where the measurement matrix is defined by

$$\boldsymbol{H}_{k|k-1} \equiv \left.\frac{\partial \boldsymbol{h}[\boldsymbol{x}(t_k), t_k]}{\partial \boldsymbol{x}}\right|_{\boldsymbol{x}=\hat{\boldsymbol{x}}_{k|k-1}} \tag{9}$$

The error covariance matrix for the state, which is defined by the conditional expectation,

$$\boldsymbol{P}_{k|k} \equiv E\{[\boldsymbol{x}(t_k) - \hat{\boldsymbol{x}}_{k|k}][\boldsymbol{x}(t_k) - \hat{\boldsymbol{x}}_{k|k}]^{\mathrm{T}} \mid \boldsymbol{z}_k\} \tag{10}$$

is updated according to the following equation:

$$\boldsymbol{P}_{k|k} = \boldsymbol{P}_{k|k-1} - \boldsymbol{K}_k\boldsymbol{H}_{k|k-1}\boldsymbol{P}_{k|k-1} = [\boldsymbol{I} - \boldsymbol{K}_k\boldsymbol{H}_{k|k-1}]\boldsymbol{P}_{k|k-1}[\boldsymbol{I} - \boldsymbol{K}_k\boldsymbol{H}_{k|k-1}]^{\mathrm{T}} + \boldsymbol{K}_k\boldsymbol{R}_k\boldsymbol{K}_k^{\mathrm{T}} \tag{11}$$

Propagation Stage

Just after the time t_k, the best estimate of the orbital elements is given by the vector $\hat{\boldsymbol{x}}_{k|k}$. Just before the next update, at time t_{k+1}, the best estimate of the state is obtained from

$$\hat{\boldsymbol{x}}_{k+1|k} = \hat{\boldsymbol{x}}_{k|k} + \int_{t_k}^{t_{k+1}} \boldsymbol{f}[\hat{\boldsymbol{x}}_{k|k}, t]\, dt \tag{12}$$

According to our model, only the last element of the state is changing. In practice the continuous form of Eq.(12) is used and integrated using the fourth-order Runge-Kutta (RK4) method [12],

$$\dot{\hat{\boldsymbol{x}}}(\tau / t_k) = \boldsymbol{f}[\hat{\boldsymbol{x}}(\tau / t_k), \tau] \tag{13}$$

where $\hat{\boldsymbol{x}}(\tau / t_k)$ is the state estimate at the epoch time τ, which belongs to the interval $[t_k, t_{k+1})$.

We propagate the covariance matrix according to

$$\boldsymbol{P}_{k+1|k} = \Phi_k \boldsymbol{P}_{k|k} \Phi_k^{\mathrm{T}} + \int_{t_k}^{t_{k+1}} \Phi_k \boldsymbol{G}(\tau)\boldsymbol{Q}(\tau)\boldsymbol{G}^{\mathrm{T}}(\tau)\, \Phi_k^{\mathrm{T}}\, d\tau \tag{14}$$

where

$$\Phi_k = \Phi[\tau, t_k; \hat{\boldsymbol{x}}(\tau / t_k)] \tag{15}$$

is the transition matrix from the state at time t_k to the state at time τ . The state transition matrix satisfies the differential equation,

$$\frac{d\Phi[\tau,t_k;\hat{\boldsymbol{x}}(\tau/t_k)]}{d\tau} = \boldsymbol{F}[\tau;\hat{\boldsymbol{x}}(\tau/t_k)]\Phi[\tau,t_k;\hat{\boldsymbol{x}}(\tau/t_k)] \tag{16}$$

with initial condition

$$\Phi[t_k,t_k;\hat{\boldsymbol{x}}(t_k/t_k)] = \boldsymbol{I} \tag{17}$$

and where

$$\boldsymbol{F}[\tau;\hat{\boldsymbol{x}}(\tau/t_k)] \equiv \left.\frac{\partial \boldsymbol{f}[\boldsymbol{x},\tau]}{\partial \boldsymbol{x}}\right|_{\boldsymbol{x}=\hat{\boldsymbol{x}}(\tau/t_k)} \tag{18}$$

According to Eq.(4) where the function $\boldsymbol{f}[\boldsymbol{x},\tau]$ is defined, Eq.(18) is determined by the (6×6) matrix

$$\boldsymbol{F}[\tau;\hat{\boldsymbol{x}}(\tau/t_k)] = \left[\begin{array}{cccccc} 0 & \cdots & \cdots & \cdots & \cdots & 0 \\ \vdots & & & & & \vdots \\ 0 & \cdots & \cdots & \cdots & \cdots & 0 \\ \dfrac{\partial f_6}{\partial a} & \dfrac{\partial f_6}{\partial e} & 0 & 0 & 0 & \dfrac{\partial f_6}{\partial \nu} \end{array}\right]_{\boldsymbol{x}=\hat{\boldsymbol{x}}(\tau/t_k)} \tag{19}$$

For the calculation of the state transition matrix in Eq.(16), the function $\boldsymbol{F}[\tau;\hat{\boldsymbol{x}}(\tau/t_k)]$ is assumed constant over the time step of integration $h = t_{k+1} - t_k$. Thus we can approximate the solution of the differential equation by

$$\Phi[t_{k+1},t_k;\hat{\boldsymbol{x}}(\tau/t_k)] \cong \sum_{n=0}^{\infty} \frac{(t_{k+1}-t_k)^n}{n!}\, \boldsymbol{F}^{(n)}[t_k;\hat{\boldsymbol{x}}(\tau/t_k)] \tag{20}$$

which gives at the first order

$$\Phi[t_{k+1},t_k;\hat{\boldsymbol{x}}(\tau/t_k)] \cong \boldsymbol{I} + (t_{k+1}-t_k)\boldsymbol{F}[t_k;\hat{\boldsymbol{x}}(\tau/t_k)] \tag{21}$$

or

$$\Phi[t_k+h,t_k;\hat{\boldsymbol{x}}(\tau/t_k)] \cong \boldsymbol{I} + h\,\boldsymbol{F}[t_k;\hat{\boldsymbol{x}}(\tau/t_k)] \tag{22}$$

From Eq.(22) the integral term in Eq.(14) is written as

$$\Phi_k \boldsymbol{G}(t)\boldsymbol{Q}(t)\boldsymbol{G}^{\mathrm{T}}(t)\,\Phi_k^{\mathrm{T}} = \boldsymbol{G}\boldsymbol{Q}\boldsymbol{G}^{\mathrm{T}} + h(\boldsymbol{F}\boldsymbol{G}\boldsymbol{Q}\boldsymbol{G}^{\mathrm{T}} + (\boldsymbol{F}\boldsymbol{G}\boldsymbol{Q}\boldsymbol{G}^{\mathrm{T}})^{\mathrm{T}}) + h^2\,\boldsymbol{F}\boldsymbol{G}\boldsymbol{Q}\boldsymbol{G}^{\mathrm{T}}\boldsymbol{F}^{\mathrm{T}} \tag{23}$$

Assuming that the integration interval is small enough to consider $\boldsymbol{G}$ and $\boldsymbol{Q}$ constant over the integration interval and neglecting the term in h^2 , we have

$$\int_{t_k}^{t_{k+1}} \Phi_k \boldsymbol{G}(\tau)\boldsymbol{Q}(\tau)\boldsymbol{G}^{\mathrm{T}}(\tau)\Phi_k^{\mathrm{T}}\, d\tau \cong h\,\boldsymbol{G}\boldsymbol{Q}\boldsymbol{G}^{\mathrm{T}} \tag{24}$$

In Eq.(3) the noise input matrix $\boldsymbol{G} = \boldsymbol{I}$. The covariance propagation equation (Eq.(14)) becomes

$$\boldsymbol{P}_{k+1|k} = (\boldsymbol{I} + h\,\boldsymbol{F}[t_k;\hat{\boldsymbol{x}}(\tau/t_k)])\boldsymbol{P}_{k|k}(\boldsymbol{I} + h\,\boldsymbol{F}[t_k;\hat{\boldsymbol{x}}(\tau/t_k)])^{\mathrm{T}} + \boldsymbol{Q}_k \tag{25}$$

where

$$\boldsymbol{Q}_{\mathrm{k}} = h\,\boldsymbol{Q} \tag{26}$$

SIMULATION TESTS AND RESULTS

The simulated data were produced using the orbit model described in section 2 and a 8th-order geomagnetic field model based on the WMM2005 model[3] was used to generate the measured magnetic field onboard the satellite. A zero-mean white noise with a standard deviation of 200 nT was added to each component of the magnetic field. The tests were realized with a LEO satellite having a semi-major axis of 6985 km, which gives a period (for one revolution) of about 97 min. Different values of inclination and eccentricity were tested. The sampling time interval (or the time between two measurements) was chosen equal to 30 s.

The first test was realized with an inclination of 53 deg and an almost circular orbit with an eccentricity close to zero. The position estimation error obtained is plotted in Figure 2 and the velocity estimation error is in Figure 3. The initial errors of this test were 550 km on the position and 605 m/s on the velocity. The algorithm converges approximately after 7 revolutions to an averaged steady-state error of about 15 km. The satellite velocity estimation error converges to an average of about 18 m/s. The semi-major axis estimation error is plotted in Figure 4 and converges slowly to a value around zero.

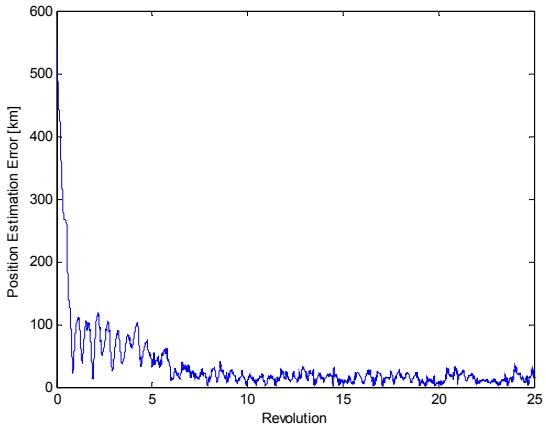

Figure 2: Position estimation error (i=53 deg, e≈0).

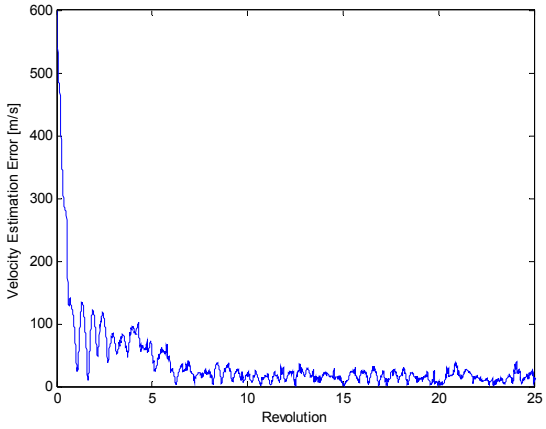

Figure 3: Velocity estimation error (i=53 deg, e≈0).

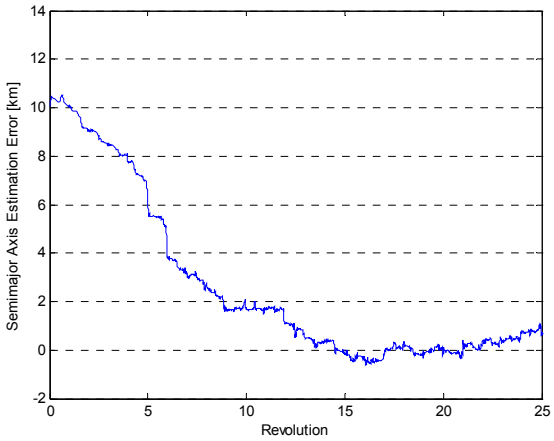

Figure 4: Semi-major axis estimation error (i=53 deg, e≈0).

In the second test we changed only the inclination to obtain a near-equatorial orbit, with i = 2 deg. The result for the position error is plotted in Figure 5. We noticed that the rapidity of converge is comparable but the steady-state error increased to about 18 km. This fact will be discussed at the end of this section.

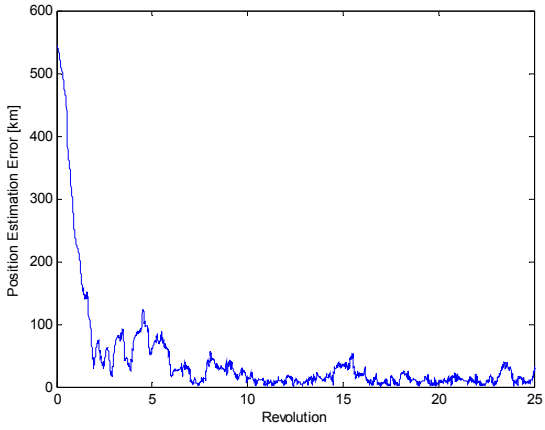

Figure 5: Position estimation error (i=2 deg, e≈0).

In the following test we considered an orbit of inclination 53 deg and eccentricity 0.5, with a larger initial error (1067 km and 1615 m/s). The result for the position estimation error is plotted in Figure 6. The improvement in the performance is considerable in terms of rapidity of convergence (2.5 orbits) and average steady-state value (about 6.3 km) even with a larger initial error. The degradation of the filter performances when the orbit is almost circular is due to the fact that the argument of perigee ω and the true anomaly ν are not defined for a circular orbit because it has no periapsis. The closer we are from the case of null eccentricity the more difficult is the determination of these two elements.

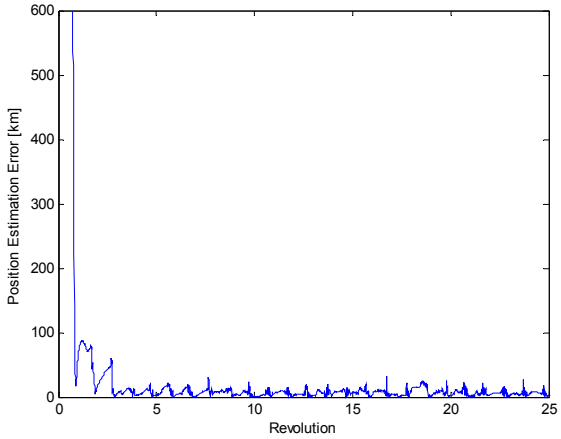

Figure 6: Position estimation error (i=53 deg, e=0.5)

To better examine the influence of a near-equatorial orbit on the filter performance we chose to simulate the case where i = 2 deg and e = 0.5, which does not present the difficulty of observing the state element ω and ν. The results are shown on Figs. 7 and 8. The convergence is rapid but the average steady state, close to 11.3 km, is almost twice higher than in the previous case (where i was 53 deg).

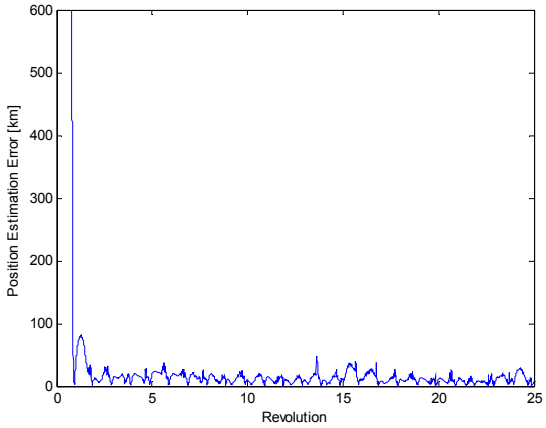

Figure 7: Position estimation error (i=2 deg, e=0.5).

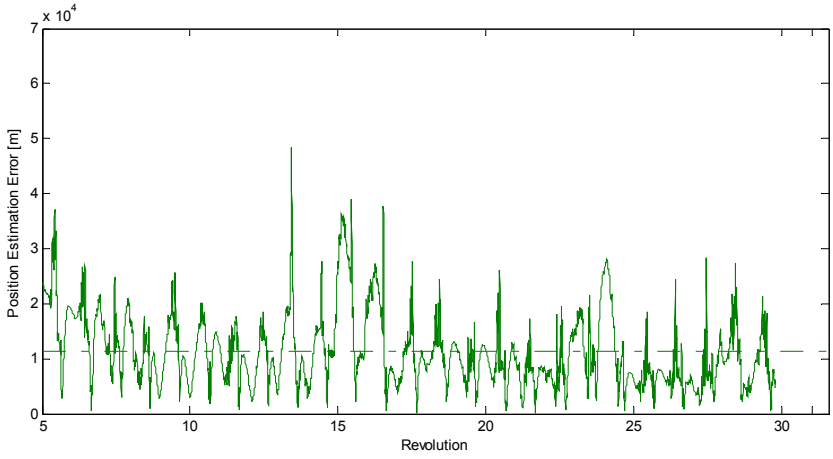

Figure 8: Position estimation error: Steady-state and average (i=2 deg, e=0.5).

This deterioration in the filter performance when we used near-equatorial orbits was predictable and is due to the limited variation of the magnetic field vector along these orbits. A plot of the Earth's magnetic field vector is shown in Figure 9 to support this statement.[4]

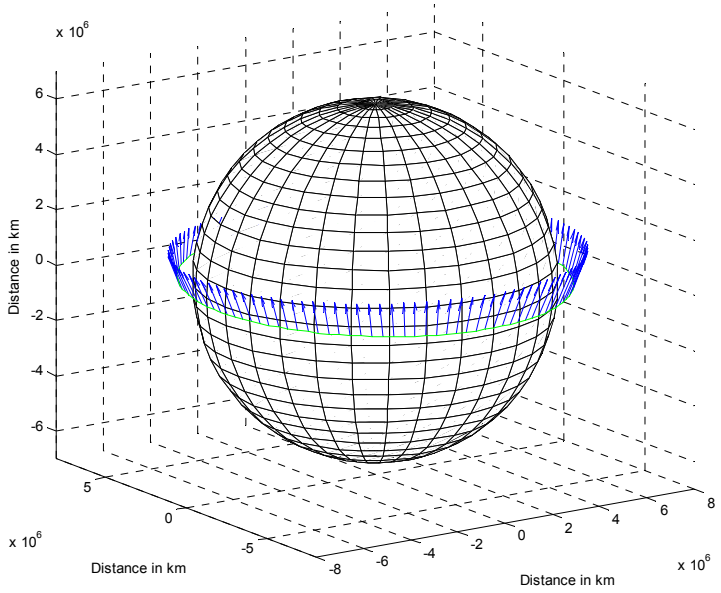

Figure 9 Earth's magnetic field vector along a circular orbit inclined of 2 degrees.

CONCLUSIONS

The estimation of a satellite orbital position at low altitude from only magnetometer measurements is possible. The state of the filter is using the classical orbital elements and the implementation is based on the EKF algorithm.

The test results have shown the influence of the inclination and eccentricity of the orbit on the filter performance. Lowering the eccentricity (near-circular orbit) increases the time of convergence and the average steady-state value for the estimation of the position (and velocity) of the satellite. The average steady-state value for the position has more than doubled if we compare Figure 2 with Figure 6. Lowering the inclination, to simulate near-equatorial orbits, did not seem to have an effect on the rapidity of convergence of the filter (see Figure 6 and Figure 7), but it did worsen the steady-state value that went from 6.3 km with an inclination of 53 deg to 11.3 km with an inclination of 2 deg.

To improve the estimation accuracy of the satellite position in near-circular or circular orbit requires modifying the elements chosen in the filter state. The argument of perigee and the true anomaly can be replaced by their sum to represent a new variable called argument of latitude in Ref. 10.

REFERENCES

[1] Tapley, B. D., Ries, J. C., Davis, G. W. and Eanes, R. J., (1994) Precision orbit determination for TOPEX/POSEIDON, *Journal of Geophysical Research*, Vol. 99.

[2] Irish, K., Gold, K., Born, G., Reichert, A. and Axelrad, P., (1998) Precision Orbit Determination for the Geosat Follow-On Satellites, *Journal of Spacecraft and Rockets*, Vol. 35, pp. 336-341.

[3] McLean, S., Macmillan, S., Maus, S., Lesur, V., Thomson, A. and Dater, D., (2004) *The US/UK World Magnetic Model for 2005-2010*, Dec. 2004, NOAA Technical Report NESDIS/NGDC-1.

[4] Filipski, M.N. and Renuganth, V., (2005) Geomagnetic Field Analysis for Optimized Measurement by a Nanosatellite in an Equatorial Orbit, *International Conference on Cutting-Edge Space Technologies*, Langkawi, Malaysia, Dec. 2005.

[5] Psiaki, M.L. and Martel, F., (1989) Autonomous Magnetic Navigation for Earth Orbiting Spacecraft, *Proceedings of the 3rd Annual AIAA/USU Conf. on Small Satellites*, Sept. 1989, Logan, Utah.

[6] Shorshi, G. and Bar-Itzhack, I.Y., (1995) Satellite Autonomous Navigation Based on Magnetic Field Measurements, *Journal of Guidance, Control, and Dynamics*, Vol. 18, No. 4, pp.843-850.

[7] Challa, M., Natanson, G. and Wheeler, C., (1996) Simultaneous determination of spacecraft attitude and rates using only a magnetometer, *AIAA/AAS Astrodynamics Conference*, San Diego, CA, AIAA-1996-3630.
[8] Psiaki, M.L. and Oshman, Y., (2003) Spacecraft Attitude Rate Estimation From Geomagnetic Field Measurements, *Journal of Guidance, Control and Dynamics*, Vol. 26, No. 2, pp. 244-252.
[9] Humphreys, H., Psiaki, M., Klatt, E., Powell, S. and Kintner, P., (2004) Magnetometer-based Attitude and Rate Estimation for a Spacecraft with Wire Booms, *AIAA Guidance, Navigation, and Control Conference and Exhibit*, Providence, Rhode Island, AIAA-2004-5338.
[10] Vallado, D.A., (2001) *Fundamentals of Astrodynamics and Applications*, 2nd Ed., Space Technology Library, Kluwer Academic Publishers, Dordrecht, Holland.
[11] Gelb, A., (1982) *Applied Optimal Estimation*, MIT Press, Cambridge, MA.
[12] Arfken, G., (1985) *Mathematical Methods for Physicists, 3rd ed.* Orlando, FL: Academic Press, pp. 492-493.